

Frequency Response Estimation of 1.3 μm Waveguide Integrated Vertical PIN Type Ge-on-Si Photodetector Based on the Analysis of Fringing Field in Intrinsic Region

Dongjun Seo¹, Won-Bae Kwon², Sung Chang Kim², and Chang-Soo Park^{1*}

¹*School of Electrical Engineering and Computer Science, Gwangju Institute of Science and Technology (GIST),
Gwangju 61005, Korea*

²*Honam Research Center, Electronics and Telecommunications Research Institute (ETRI),
Gwangju 61012, Korea*

(Received October 14, 2019 : revised October 22, 2019 : accepted October 22, 2019)

In this paper, we introduce a 1.3- μm 25-GHz waveguide-integrated vertical PIN type Ge-on-Si photodetector fabricated using a multi-project wafers service based on fringing field analysis in the depletion region. In general, 1.3- μm photodetectors fabricated using a commercial foundry service can achieve limited bandwidths because a significant amount of photo-generated carriers are located within a few microns from the input along the device length, and they are influenced by the fringing field, leading to a longer transit time. To estimate the response time, we calculate the fringing field in that region and the transit time using the drift velocity caused by the field. Finally, we compare the estimated value with the measured one. The photodetector fabricated has a bandwidth of 20.75 GHz at -1 V with an estimation error of <3 GHz and dark current and responsivity of 110 nA and 0.704 A/W, respectively.

Keywords : Silicon photonics, Germanium PIN photodetectors, Fringing field, Response time
OCIS codes : (040.3060) Infrared; (060.4510) Optical communication; (230.5160) Photodetectors

I. INTRODUCTION

Over the past few decades, high-speed waveguide-integrated Ge photodetectors based on silicon photonics have become popular in the area of integrated optics because they can easily be coupled to electronic components as a one-chip solution. Further, they offer the advantage of using a well-stabilized CMOS-like fabrication process [1] as well as fabless fabrication at low cost [2-6]. However, as far as a multi-project wafers (MPW) service utilizing a standardized Ge layer is concerned, it is not easy to obtain photodetectors with bandwidths of more than 20 GHz at a wavelength of 1.3 μm . This is so because a significant quantity of photo-generated carriers are distributed within the first micron length of the Ge layer and photo-generated carriers are influenced by the weak fringing field, not by the internal field formed over the depletion region. Thus, it takes a longer time for the carriers to transit the region. For this

reason, photodetectors using a Ge layer or a III-V compound under private fab facility have mostly been reported. H. Chen *et al.* reported a lateral PIN type photodetector that performs the frequency response of >50 GHz at -2 V using a very thin (160 nm) Ge layer at 1.3 μm [7]. D. Inoue *et al.* demonstrated 10 Gb/s operation of InGaAs quantum dot PIN photodetector directly grown on Si (001) at 1.3 μm , showing the performance with the responsivity of 0.08 A/W and the bandwidth of 5.5 GHz at -5 V, respectively [8]. Also, Y. S. Wang *et al.* introduced InGaAs PIN photodetector formed of planar buried heterostructure with the bandwidth of 12.4 GHz at -5 V [9]. However, even in photodetectors using MPW service, fast frequency response could be achieved by estimating the bandwidth in the design stage.

In this paper, we introduce a method to estimate the bandwidth of photodetectors using fabless fabrication for a 1.3- μm application. The bandwidth is determined by the response time of the PIN photodetector to incident light,

*Corresponding author: msp@gist.ac.kr, ORCID 0000-0002-0130-6648

Color versions of one or more of the figures in this paper are available online.



This is an Open Access article distributed under the terms of the Creative Commons Attribution Non-Commercial License (<http://creativecommons.org/licenses/by-nc/4.0/>) which permits unrestricted non-commercial use, distribution, and reproduction in any medium, provided the original work is properly cited.

which is mostly limited by the transit time for the photo-generated carriers to be extracted to both electrodes. Therefore, by calculating the drift time of the carriers far away from the n^{++} -doped Ge layer in the depletion region of the PIN structure, we can estimate the bandwidth of the photodetector to be fabricated. The field and absorption analysis are executed based on the finite-difference time-domain (FDTD) method using simulation tools from Lumerical Inc, Canada. The photodetector to be tested is fabricated by the MPW service of IME A*Star, Singapore. Finally, the bandwidth measured is compared with the estimated bandwidth with the applied voltage.

II. DEVICE STRUCTURE

Figure 1 shows the photodetector that is usually considered for commercial foundry service. The device was based on a 220-nm-thick silicon-on-insulator platform that has a 2- μm -thick buried oxide layer. The PIN structure consisted of p^+ - and p^{++} -doped Si layers (p^+ - and p^{++} -Si layers), an intrinsic Ge layer (i -Ge layer), and an n^{++} -doped Ge layer (n^{++} -Ge layer). The whole silicon slab was p^+ -doped and areas located under the electrodes were p^{++} -doped for reducing diffusion time. The maximum doping concentrations of p^+ , p^{++} , and n^{++} were 3.5×10^{19} , 5×10^{20} , and $1.27 \times 10^{21} \text{ cm}^{-3}$, respectively. The width and length of the Ge layer were chosen as 8 μm each to obtain almost 90% light absorption efficiency.

Using an FDTD tool, 3-dimensional simulation was conducted at temperature of 300 K. Minimum mesh step was 0.25 nm which was sufficiently small for reflecting every structural changes of our design. Every edge boundary was set as an 8-layer Perfectly Matched Layer boundary to absorb any reflected light beam at the edge of the simulation region in such a way not to go back to the germanium. An anti-symmetric boundary was also used in the x-direction to reduce simulation time. It could be used by taking advantage of the symmetric characteristic of the optical mode and light propagation in the x-direction. The mode source was used as a light source, which generates the fundamental mode, obviously the TE mode in our structure, in the wavelength of 1.3 μm (absorption efficiency in O-band wavelengths was not very different). Doping profiles were

imported to FDTD simulation from DEVICE solution (Lumerical Inc.).

The simulated light absorption efficiency was obtained as 89% at a wavelength of 1.3- μm using coupling waveguide dimensions of thickness 220 nm and width 380 nm. The length of the n^{++} -Ge layer should also be 8 μm . However, the actual length turned out to be 6.5 μm owing to difficulties encountered by the foundry service in fabrication.

Figure 2 shows the carrier generation rate inside the intrinsic Ge layer based on light absorption at a wavelength of 1.3- μm . $\text{Re}(G)$ refers to the real value of the generation rate. The averaged generation rate is also shown in Fig. 2(a) and 89%, 95%, and 98% of the total amount of generated carriers were distributed within widths of 3, 4, and 5 μm , respectively. Therefore, we chose the n^{++} -Ge layer with the width of 5 μm to absorb as many carriers as possible. Figure 2(b) shows light absorption along the device length, i.e., along the traveling direction, and most carriers are absorbed over a few microns. However, the starting position of the n^{++} -Ge layer is placed 0.75 μm away from the input side owing to the fabrication restriction shown in Fig. 1(c). Approximately 41% of the incident light is absorbed in this undoped region and the carriers are drifted by the fringing field between the n^{++} -Ge layer and the p^+ -Si layer.

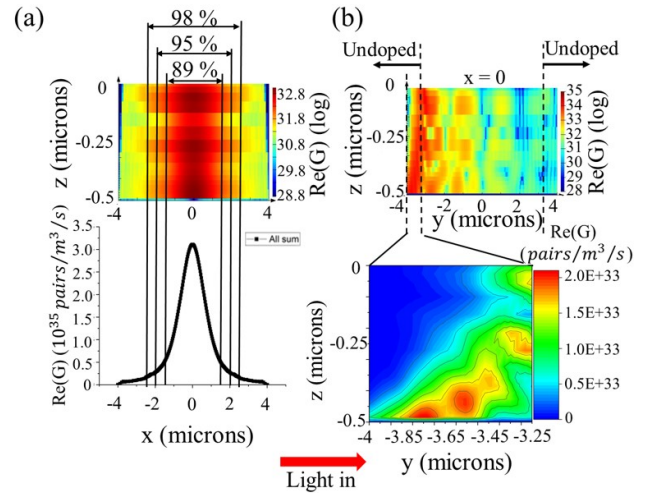


FIG. 2. Simulated carrier generation rate-(a) front view; (b) side view.

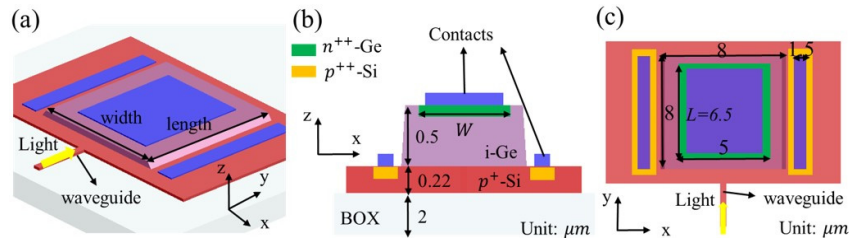


FIG. 1. Photodetector structure diagrams-(a) perspective view; (b) front view; (c) top view.

III. FRINGING FIELD ANALYSIS

The bandwidth of a photodetector is determined by the response time (τ_r) of the device, which is defined as the time that it takes for the output current to reach from 10% to 90% of the steady-state current when the step optical input is applied. The response time depends on three independent parameters—RC time constant (τ_{RC}), drift time (τ_{drift}) in the space-charge region, and diffusion time (τ_{diff}) in the charge-neutral region, as follows [10]:

$$\tau_r = \sqrt{(2.2\tau_{RC})^2 + \tau_{drift}^2 + \tau_{diff}^2}, \quad (1)$$

where the multiplier 2.2 comes from the fact that the rise time of the RC circuit to the applied step function is influenced exponentially by the RC time constant and given by the time corresponding to 10% to 90% of the final value. The diffusion time is negligible in the case of a fully depleted condition with relatively high reverse bias voltage [11]. Thus, the response time is mainly determined by the drift time and RC time constant. The drift time is impacted by the drift velocity and traveling distance of the carriers, which are decided by the magnitude and shape of the electric-field flux distribution.

Figure 3 shows two identical plates that form a capacitor on the y - z plane at $x=0$. The two plates are separated by distance d , and the width and length are W and L , respectively. The potential difference between the two plates

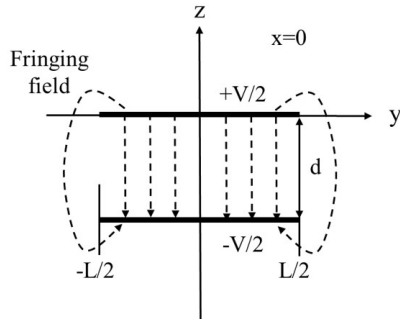


FIG. 3. Diagram of rectangular parallel plate capacitor in y - z plane at $x=0$.

is V . The curved electric field outside the two plates is referred to as the fringing field. G. W. Parker derived the electrical potential function of the fringing field for a parallel rectangular plate capacitor with arbitrary W and L in 2002 [12]. The electrical potential function Φ at $x=0$ is given by

$$\Phi(0, y, z) = \frac{V}{2\pi} \left\{ \arctan \left[\frac{W(L-2y)}{2zD_-} \right] + \arctan \left[\frac{W(L+2y)}{2zD_+} \right] \right\}, \quad (2)$$

where

$$D_{\pm} = \sqrt{W^2 + (L \pm 2y)^2 + 4z^2}. \quad (3)$$

By applying the relation $E = -\nabla\Phi$ to Eq. (2), the y - and z -directional electric fields E_y and E_z at $x=0$ are given by

$$E_y(0, y, z) = \frac{-2V}{\pi} \left\{ \frac{zW(L-2y)^2 - D_-^2}{4z^2D_-^3 + W^2(L-2y)^2D_-} + \frac{zW(L+2y)^2 - D_+^2}{4z^2D_+^3 + W^2(L+2y)^2D_+} \right\}, \quad (4)$$

$$E_z(0, y, z) = \frac{V}{\pi} \left\{ \frac{W(L-2y)(D_-^2 + 4z^2)}{4z^2D_-^3 + W^2(L-2y)^2D_-} + \frac{W(L+2y)(D_+^2 + 4z^2)}{4z^2D_+^3 + W^2(L+2y)^2D_+} \right\} \quad (5)$$

This result can be extended to areas where $x \neq 0$ within the plate width range in sufficiently small structures.

Figure 4 shows the distribution of the electric field in the region not covered by the n^+ -Ge layer. Figure 4(a) shows the flow of the carriers drifted by the fringing field in the region. Figures 4(b) and 4(c) show the contours of the electric field calculated using Eqs. (4) and (5). As we can see, the two layers, of n^{++} -Ge and p^+ -Si, act like a pair of rectangular parallel plates of a capacitor when bias voltage is applied. These two layers generate an internal field between them as well as a fringing field outside the n^{++} -Ge layer. According to previous results with respect to photo-generated carriers, 40% of the carriers were generated outside the n^{++} -Ge layer and impacted by the fringing field as shown in Fig. 4(a). Finally, the response time related to the transition across the two layers is determined by the carriers far away from the n^{++} -Ge layer (point A in the model shown in Fig. 4(a)). First, we calculated the y - and z -directional fringing field magnitudes (E_y and E_z) on the y - z plane using Eqs. (4) and (5) for the case of W , L , and

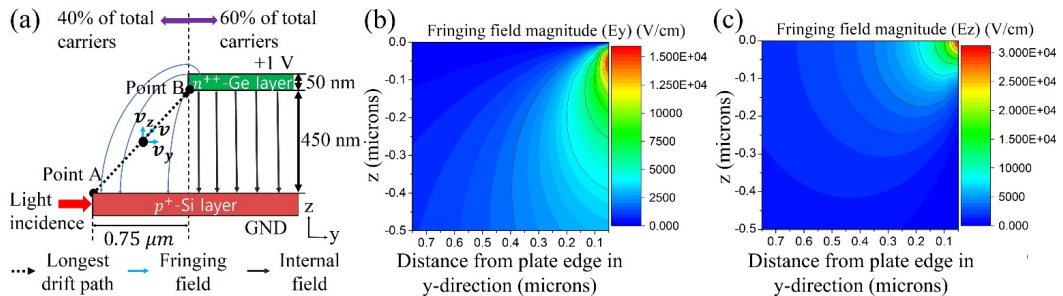


FIG. 4. Fringing field analysis model and contour plots of fringing field magnitude ($W = 5 \mu\text{m}$, $L = 6.5 \mu\text{m}$)—(a) analysis model; (b) y -direction component (E_y) contour plot; (c) z -direction component (E_z) contour plot.

V equal to 5 μm , 6.5 μm , and 1 V, respectively. The field magnitudes were plotted along the device length starting from 0.05 (close to the n^{++} -Ge layer) to 0.75 μm (light input side). From Fig. 2(b), the incident optical power was mainly absorbed over the edge region when the device operates at 1.3 μm . Furthermore, as shown in Fig. 4(a), the p^+ layer was extended to the front side (light input) and, on the other hand, the n^{++} layer was not due to the limitation in the MPW process. Therefore, the carriers moving along the path of point A and B experience the longest transit time. The distance between the p^+ layer and the n^{++} layer was 450 nm (Ge growing was over 500 nm on top of p^+ layer and then the depth of the n^{++} -Ge layer was 50 nm using the 170-keV phosphorus implantation model with an ion dose of $5 \times 10^{16} \text{ cm}^{-2}$) [13]. To obtain the transit time, we used the relation between the electron drift velocity and the applied electric field, derived and experimentally proved, based on the Monte Carlo program with a physical model of the band structure and the scattering mechanism of electrons in Ge [14]. The saturation velocity of an electron in germanium is $6.5 \times 10^6 \text{ cm/s}$. The electron drift velocity was distinguished as v_x , v_y , and v_z depending on the following directions—path, y -axis, and z -axis, respectively. To calculate transit time, we divided the drift path length into 10 sub-paths by intersecting the electric field contour lines. For simplicity of calculation, we ignored the time taken to accelerate using the fact that the acceleration will be relatively high (approximately $1.76 \times 10^{18} \text{ cm/s}^2$ for 1 kV/m) compared to the variation in the drift velocity between the sub-paths. The calculation results are represented in Table 1. Therefore, the drift time was estimated to be approximately 14.68 ps.

Further, the capacitance effect owing to the fringing field must be considered as a factor limiting the frequency response of the photodetector. In general, the junction capacitance is determined by considering only the internal electric field between the two rectangular plates. However,

in our case, depending on the fringing field, the capacitance effect must also be considered for exact analysis. Using Palmer's model [15], the capacitance of a rectangular parallel plate capacitor is given by

$$C = \frac{\epsilon WL}{d} \left\{ 1 + \frac{d}{\pi W} \left[1 + \ln \left(\frac{2\pi W}{d} \right) \right] \right\} \left\{ 1 + \frac{d}{\pi L} \left[1 + \ln \left(\frac{2\pi L}{d} \right) \right] \right\}, \quad (6)$$

where ϵ is the permittivity of germanium. It is assumed that the electrical potential difference of the two plates is 1 V. For the dimensions $d = 0.5 \mu\text{m}$, $L = 6.5 \mu\text{m}$, and $W = 5 \mu\text{m}$, the capacitance was calculated as 12.13 fF. We assumed that the series resistance required to estimate the RC time constant was 100 Ω [3] and the load resistance was 50 Ω . Finally, using Eq. (1), the total response time was calculated as approximately 14.79 ps at -1 V. The corresponding bandwidth was estimated to be 23.66 GHz using the relation $0.35/\tau_r$, which is typically used to estimate the bandwidth in an RC circuit. In the same manner, the bandwidth at -2 V was 25.35 GHz.

IV. MEASUREMENT RESULTS

The photodetector was fabricated with the dimensions shown in Fig. 1. General fabrication process steps of PIN photodetector with MPW service were illustrated in Fig. 5. Figure 6 shows a micrograph of the fabricated device. The contact metal was formed to the GSG (ground-signal-ground) type. The device under test was fastened to the platform using the vacuum adsorption method. All measurements were conducted at 25°C. A source meter (Keithley Instruments 2400, 0.025% measurement accuracy) was used for inducing the bias voltage and measuring the output current. The carriers accumulated on the metal pad were gathered by the microwave probe (GGB industry picoprobe 40A, GSG type, 40 GHz frequency range) for conveying the output to the measuring equipment.

TABLE 1. Drift time calculation results at -1 V

Sub-path number	Sub-path length [nm]	v_y [10^6 cm/s]	v_z [10^6 cm/s]	v [10^6 cm/s]	Drift time [ps]
1	190.8	3.62	3.62	5.12	3.73
2	108	4.22	4.24	5.98	1.81
3	117.2	4.9	4.81	6.5	1.8
4	62.6	5.23	5.23	6.5	0.96
5	50	5.56	5.68	6.5	0.77
6	44.7	5.79	5.91	6.5	0.69
7	36.1	5.93	6.0	6.5	0.56
8	51.5	6.17	6.09	6.5	0.79
9	58.3	6.39	6.31	6.5	0.9
10	173.3	6.5	6.5	6.5	2.67
Total	892.5				14.68

The simulation was conducted on the x - z plane and then repeated along the device length, i.e., the y -direction. As we mentioned earlier, the photodetector fabricated has an asymmetrical structure along the y -directional length of the

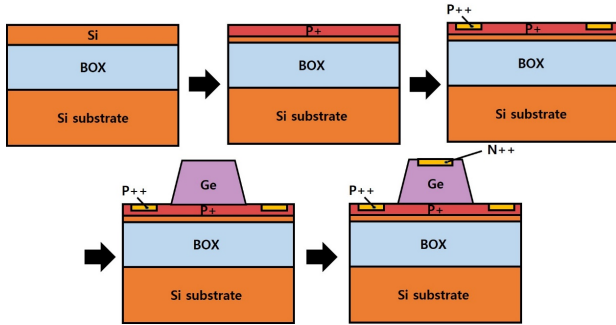


FIG. 5. Fabrication process of Ge-on-Si PIN photodiode.

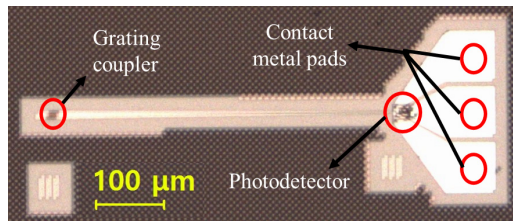


FIG. 6. Micrograph of the fabricated photodetector.

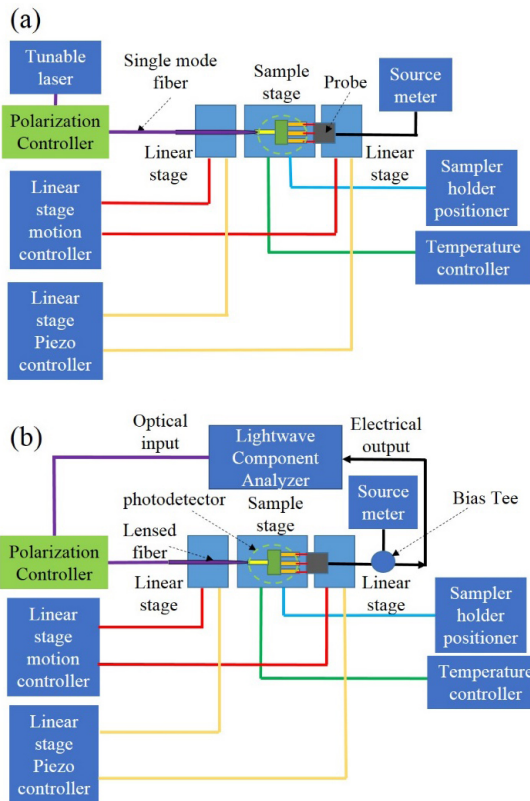


FIG. 7. The experimental setups-(a) responsivity measurement; (b) frequency response measurement.

n^{++} and p^{+} layers. However, owing to the limited capacity of the simulation tool, the structure has a symmetrical structure, i.e., the same length. The simulated responsivity to the incident optical power of 1 mW was 0.8 A/W at bias voltage of 0 to -4 V. For comparison with the simulated results, the experimental setup shown in Fig. 7 was arranged. In Fig. 7(a), a 1.3- μ m tunable laser source was used as a wavelength scanner to investigate the responsivity with wavelength. The light was coupled to the grating coupler connected to the input waveguide of the photodetector with 25% coupling efficiency using a lensed fiber. The laser output power was 0.5 mW and thus the input power to the photodetector was approximately 0.125 mW. The minimum and maximum currents from the photodetector were 0.088 mA and 0.090 mA, respectively. The corresponding responsivities were 0.704 and 0.720 A/W, respectively. The responsivity appeared to be somewhat increased with the applied voltage, which was attributed to the increase in the fringing field. Figure 8 shows the simulated (black square) and measured (red circle) responsivities as functions of the

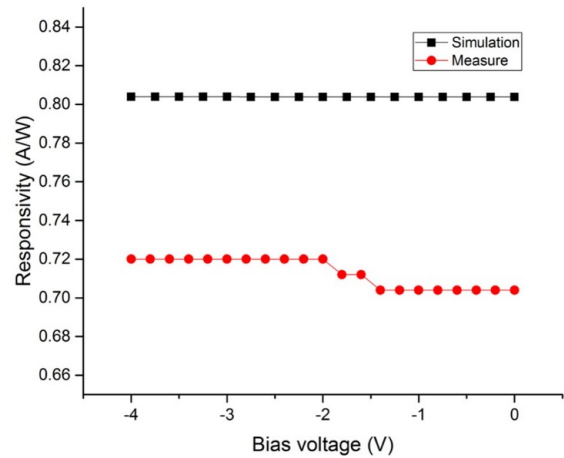


FIG. 8. Simulated and measured responsivities.

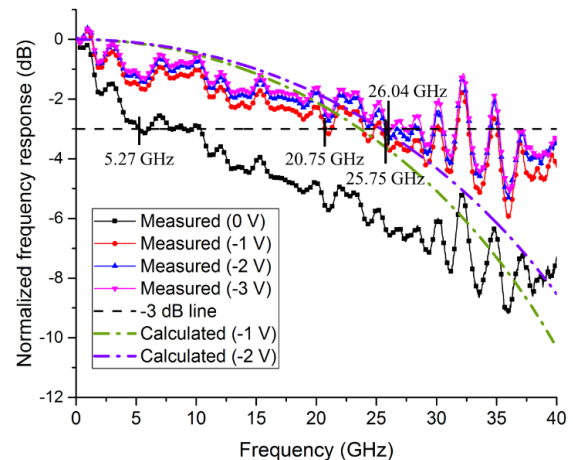


FIG. 9. Measured and calculated frequency response of the fabricated device.

applied bias voltage. The dark currents measured were about 110 nA and 200 nA at -1 V and -2 V, respectively. These values appeared to be somewhat higher due to thermionic emission through the low dislocation densities of Ge. In general, dark current density is around two orders of magnitude higher than that of InGaAs photodetectors though it has the distinct advantage of easy integration with Si over InGaAs.

Then, the frequency response was measured using the light component analyzer (Agilent LCA, N4373D, 67 GHz frequency range) and vector network analyzer (Agilent PNA, N5227A, 67 GHz frequency range) as shown in Fig. 7(b). The normalized frequency response is shown in Fig. 9. The measured bandwidths of the device at 0, -1, -2, and -3 V were 5.27, 20.75, 25.75, and 26.04 GHz, respectively. It is apparent that the bandwidth increased with an increase in the reverse bias voltage. However, the increase was not as much as in the earlier case owing to the saturation of the drift velocity. Finally, the estimated errors between the calculated and measured bandwidths were 2.91 GHz and 0.4 GHz at -1 V and -2 V, respectively.

V. CONCLUSION

We introduced and analyzed a model to estimate the response time (i.e., bandwidth) of a 1.3- μm waveguide-integrated vertical PIN-type Ge-on-Si photodetector fabricated using a multi-project wafers (MPW) service. In this process, a significant number of photo-generated carriers is distributed over the first few microns along the device length and drifted by the fringing field in the depletion region, instead of by the internal field. By calculating the transit time of the carriers far away from the n^+ -Ge layer (light input side), we estimated the bandwidth of the photodetector to be fabricated and compared it with that of the fabricated photodetector. The calculated bandwidth considering the drift time and junction capacitance was approximately 23.66 GHz and 25.35 GHz at -1 V and -2 V, respectively. The measured bandwidths of the photodetector fabricated appeared to be 20.75 GHz and 25.75 GHz and the responsivity was approximately 0.72 A/W at -2 V. This method can effectively be used as a means to estimate the bandwidth, including the fabrication conditions and dimension parameters, in fabless design.

ACKNOWLEDGMENT

This work was supported by GIST Research Institute (GRI) grant funded by the GIST in 2019 and Electronics and Telecommunications Research Institute (ETRI) grant funded by the Korean government (19ZK1120, Development of Optical Wireless Communication and Analysis Technologies under Harsh Environment).

REFERENCES

1. D. Thomson, A. Zilkie, J. E. Bowers, T. Komljenovic, G. T. Reed, L. Vivien, D. Marris-Morini, E. Cassan, L. Viot, J.-M. Fédéli, J.-M. Hartmann, J. H. Schmid, D.-X. Xu, F. Boeuf, P. O'Brien, G. Z. Mashanovich, and M. Nedeljkovic, "Roadmap on silicon photonics," *J. Opt.* **18**, 073003 (2016).
2. G. Chen, Y. Yu, X. Xiao, and X. Zhang, "High speed and high power polarization insensitive germanium photodetector with lumped structure," *Opt. Express* **24**, 10030-10039 (2016).
3. J.-M. Lee, S. H. Cho, and W.-Y. Choi, "An equivalent circuit model for a Ge waveguide photodetector on Si," *IEEE Photon. Technol. Lett.* **28**, 2435-2438 (2016).
4. H. Zhou and Y. Sun, "Size reduction of Ge-on-Si photodetectors via a photonic bandgap," *Appl. Opt.* **57**, 2962-2966 (2018).
5. Y. Zhang, S. Yang, Y. Yang, M. Gould, N. Ophir, A. E.-J. Lim, G.-Q. Lo, P. Magill, K. Bergman, T. Baehr-Jones, and M. Hochberg, "A high-responsivity photodetector absent metal-germanium direct contact," *Opt. Express* **22**, 11367-11375 (2014).
6. M. M. P. Fard, G. Cowan, and O. Liboiron-Ladouceur, "Responsivity optimization of a high-speed germanium-on-silicon photodetector," *Opt. Express* **24**, 27738-27752 (2016).
7. H. Chen, P. Verheyen, P. D. Heyn, G. Lepage, J. D. Coster, S. Balakrishnan, P. Absil, W. Yao, L. Shen, G. Roelkens, and J. V. Campenhout, "-1 V bias 67 GHz bandwidth Si-contacted germanium waveguide p-i-n photodetector for optical links at 56 Gbps and beyond," *Opt. Express* **24**, 4622-4631 (2016).
8. D. Inoue, Y. wan, D. Jung, J. Norman, C. Shang, N. Nishiyama, S. Arai, A. C. Gossard, and J. E. Bowers, "Low-dark current 10 Gbit/s operation of InAs/InGaAs quantum dot p-i-n photodiode grown on on-axis (001) GaP/Si," *Appl. Phys. Lett.* **113**, 093506 (2018).
9. Y. S. Wang, S.-J. Chang, C. L. Tsai, M.-C. Wu, Y.-Z. Chiou, S. P. Chang, and W. Lin, "10-Gb/s planar InGaAs P-I-N photodetectors," *IEEE Sens. J.* **10**, 1559-1563 (2010).
10. A. O. Goushcha and B. Tabbert, "On response time of semiconductor photodiodes," *Opt. Eng.* **56**, 097101 (2017).
11. K.-S. Park, Y.-S. Yoon, J.-M. Park, J.-Y. Kang, B.-W. Kim, I.-G. Hwang, and K.-S. No, "Estimates of the photo-response characteristics of a non-fully-depleted silicon p-i-n photodiode for the near infrared spectral range and the experimental results," *J. Korean Phys. Soc.* **50**, 1156-1162 (2007).
12. G. W. Parker, "Electric field outside a parallel plate capacitor," *Am. J. Phys.* **70**, 502-507 (2002).
13. Y. S. Suh, M. S. Carroll, R. A. Levy, M. A. Sahiner, G. Bisognin, and C. A. King, "Modeling of boron and phosphorus implantation into (100) Germanium," *IEEE Trans. Electron Devices* **52**, 91-98 (2005).
14. C. Jacoboni, F. Nava, C. Canali, and G. Ottaviani, "Electron drift velocity and diffusivity in germanium," *Phys. Rev. B* **24**, 1014-1026 (1981).
15. H. B. Palmer, "The capacitance of a parallel-plate capacitor by the schwartz-christoffel transformation," *Electr. Eng.* **56**, 363-368 (1937).